Presented at ION GNSS+ 2014, Session C5, Tampa, FL, USA, September 8-12, 2014.

# GNSS/INS/Star Tracker Integrated Navigation System for Earth-Moon Transfer Orbit

Vincenzo Capuano, Cyril Botteron, Yanguang Wang, Jia Tian, Jérôme Leclère, Pierre-André Farine
*École Polytechnique Fédérale de Lausanne (EPFL),*
*Electronics and Signal Processing Laboratory (ESPLAB), Switzerland*

## BIOGRAPHIES

**Vincenzo Capuano** is a PhD candidate in Microsystems and Microelectronics at the École Polytechnique Fédérale de Lausanne (EPFL) and doctoral assistant in the GNSS group at EPFL STI IMT ESPLAB, in Neuchâtel, Switzerland. His current research activity focuses on the GNSS use for space navigation. He received his Master of Engineering in Astronautic Engineering with full marks from the University of Rome "La Sapienza" and his Bachelor of Engineering in Aerospace Engineering with full marks cum laude from the University of Naples "Federico II".

**Dr. Cyril Botteron** is leading, managing, and coaching the research and project activities of the Global Navigation Satellite System and Ultra-Wideband and mm-wave groups at École Polytechnique Fédérale de Lausanne (EPFL). He is the author or co-author of 5 patents and over 80 publications in major journals and conferences in the fields of wireless positioning systems, GNSS-based navigation and sensing, ultra-low-power radio frequency communications and integrated circuits design, and baseband analog and digital signal processing.

**Yanguang Wang** received the Master Degree in Electronics and Signal Processing from the Xidian University, Xi'an, China, in 2007. He is currently working in the GNSS field at École Polytechnique Fédérale de Lausanne (EPFL), focusing his researches in the acquisition and tracking in high sensitivity areas, with application to hardware receivers.

**Jia Tian** received the Master Degree in Electronics and Signal Processing from China Academy of Space Technology (Xi'an), China, in 2012. He is currently working in the GNSS field at École Polytechnique Fédérale de Lausanne (EPFL), focusing his researches in the high sensitivity acquisition areas, including GPS L1, GPS L5, Galileo E1 and Galileo E5, with FPGA implementations.

**Dr. Jérôme Leclère** received the Master Degree in Electronics and Signal Processing from ENSEEIHT, Toulouse, France, in 2008, and finished his Ph.D. in the GNSS field in 2014, at EPFL, focusing his researches in the reduction of the complexity of the acquisition of GNSS signals, with application to hardware receivers, especially using FPGAs. He developed an FPGA-based high sensitivity assisted GPS L1 C/A receiver.

**Prof. Pierre-André Farine** is professor in electronics and signal processing at EPFL, and is head of the electronics and signal processing laboratory. He received the M.Sc. and Ph.D. degrees in Micro technology from the University of Neuchâtel, Switzerland, in 1978 and 1984, respectively. He is active in the study and implementation of low-power solutions for applications covering wireless telecommunications, ultra-wideband, global navigation satellite systems, and video and audio processing. He is the author or co-author of more than 100 publications in conference and technical journals and 50 patent families (more than 270 patents).

## ABSTRACT

Over the last few years, new Global Navigation Satellite System (GNSS) applications have emerged that go far beyond the original objectives of GNSS which was providing position, velocity and timing (PVT) services for land, maritime, and air applications. Indeed, today, GNSS is used in Low Earth Orbit (LEO) for a wide range of applications such as real-time navigation, formation flying, precise time synchronization, orbit determination and atmospheric profiling. GNSS, in fact, can maximize the autonomy of a spacecraft and reduce the burden and costs of network operations. For this reason, there is a strong interest to also use GNSS for High Earth Orbit or Highly Elliptical Orbit (HEO) missions. However, the use of GNSS for HEO up to Moon altitudes is still new, and terrestrial GNSS receivers have not been designed to cope with the space environment which affects considerably the GNSS receiver performance and the GNSS solution (e.g. navigation solution). The goal of our research is therefore to develop a proof of concept of a spaceborne GNSS receiver for Earth-Moon transfer orbits, assisted by Inertial Navigation System (INS), a Star Tracker and an orbital forces model to increase the navigation accuracy and to achieve the required sensitivity.

## I. INTRODUCTION

GNSS, by requiring only relatively inexpensive realization and installation cost of the on-board GNSS receiver, with low power consumption, limited mass and volume, can maximize the autonomy of spacecraft and reduce the burden and costs of network operations. From several references such as [1], [2] and [3], theoretically, GNSS signals can be acquired and tracked even on the Moon surface, but not with the current technology. In recent years, several solutions for the use of GNSS technology at Moon altitude have been proposed (see, e.g., [2], [3]). In this paper, we propose a multi-sensor GNSS receiver integration to provide an innovative and attractive GNSS-based autonomous and flexible navigation system for HEO and for Earth-Moon orbit transfers, which usually rely on expensive Earth ground stations and complex on board systems.

**Section II** of this paper describes briefly the mission scenario taken into consideration. In particular, the reference kinematics of the space receiver is defined and the selection of the GNSS signals to be used for such mission is discussed. In order to define the required receiver performances, the first part of our study focuses on the investigation of the GNSS signals characteristics in a very highly elliptical Earth-Moon transfer Orbit from 600 km Earth altitude, in terms of signals power levels, Doppler shifts, Doppler rates and geometry factors.

**Section III** reports part of the obtained results of our analysis. Similar studies with analogue results have also been published in [4], [5]. [6] and [7].

**Section IV** describes the overall architecture of the GNSS/INS/Star Tracker integrated system that has been designed for the considered space scenario. The described integrated system is currently under development and this paper describes only the first results obtained in the first months of our research activity. In particular, our current work includes the development of a high sensitivity GPS L1/L5 receiver implemented in a FPGA and of an integrated GPS/INS/Star Tracker navigation algorithm implemented on a separate system (currently a computer). Indeed, considering all the possible aiding and supportive systems to achieve higher sensitivity, and also to increase the high dynamics tolerance and the navigation performance, an INS, a Star Tracker and orbital forces model assistance have been selected. Contrary to other similar studies (e,g. see [3]), we are not taking into consideration any kind of network assistance in order to make the integrated system as flexible and autonomous as possible. Instead, the high sensitivity GNSS receiver is "ultra tightly" integrated with the INS, because their synergistic integration overcomes their individual drawbacks and provides a more accurate and robust navigation solution than either could achieve on its own. A Star Tracker is also integrated to support the INS rotational propagation and to provide an accurate attitude estimation as well. Furthermore, an orbital forces model filters the measurements.

**Section V** and **VI** respectively present the adopted acquisition and tracking strategies and discuss briefly the GNSS aiding benefits in the acquisition and in the tracking domain, provided by the supportive systems.

**Section VII** describes the GNSS/INS/Star Tracker integration in the pseudorange and pseudorange rate domain and outlines the integration to an orbital forces model (orbital filter) currently under development. **Section VIII** reports the acquisition, tracking and navigation preliminary performance as a result of the first step of our research project.

## II. DESCRIPTION OF THE MISSION SCENARIO

### Reference Kinematics

Although several Earth-Moon trajectories are possible, for our study, the initial position and velocity of the spacecraft in terms of the (Keplerian) orbital parameters has been defined (see Table 1) to represent a simple orbit with apogee at the distance of the Moon from the Earth. The motion of the spacecraft is propagated by Spirent's SimGEN software from the initial condition as a function of perturbing accelerations (such as gravitational effects from the Earth, Sun and Moon, solar radiation pressure and atmospheric drag). Half of the corresponding osculating orbit (see Figure 1) can roughly represent an Earth-Moon transfer orbit of approximately 5 days duration. Such orbit, strongly highly elliptical, is characterized by very high dynamics and strong GNSS signals at the positions close to the perigee and relatively low dynamics and very weak GNSS signals close to the apogee (approximately at the Moon altitude). Figure 2 shows the first 14 h of this orbit, together with the GPS constellation.

**Table 1: Keplerian orbital parameters of the considered orbit.**

| Orbital Parameters | Value |
|---|---|
| Apogee | 384 000 km |
| Perigee altitude | 600 km |
| Inclination | 31° |
| Argument of Perigee | 0° |
| Right ascension of the ascending node (RAAN) | 0° |
| True Anomaly | 0° |

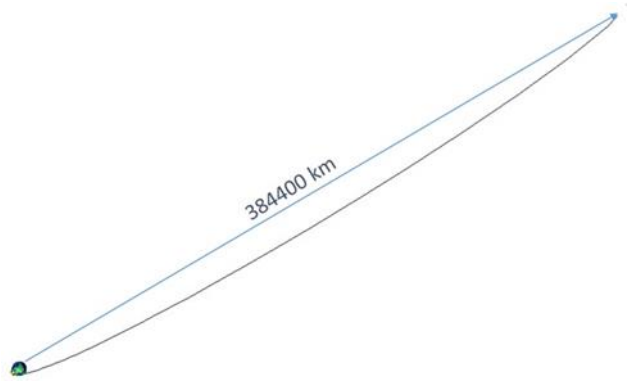


**Figure 1: Plot of half orbit defined in Table 1.**

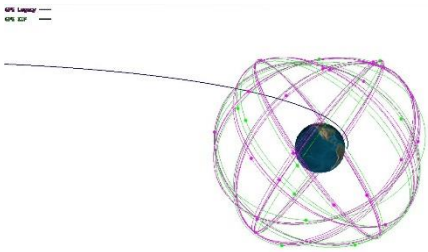

**Figure 2: Plot of the first 14 h of the defined orbit and of the GPS constellation.**

### GNSS Signals Selection

The selection of the GNSS signals to be used for such a mission depends on several criteria, such as the number of signals available from a given constellation, the targeted Geometric Dilution of Precision (GDOP), the targeted ranging accuracy, and the acceptable receiver complexity for receiving and processing the signals.

First, regarding the frequency band, the L1/E1 (1575.42 MHz) and the L5/E5 (1176.45 MHz) bands have been selected as the most interesting for such a mission, since the four GNSS (i.e., GPS, GLONASS, Galileo, and BeiDou) transmit or plan to transmit in these bands. Moreover, both L1/E1 and L5/E5 can be used to eliminate the first order ionosphere effects (99.9 %) on code and carrier-phase measurements [8]. Second, regarding the GDOP, it is much better to use signals from two or more systems rather than from only one. For example, [5] and [7] show a reduction of the GDOP by a factor greater than two for a GPS-Galileo receiver compared to a GPS receiver in HEO. Third, the signals in the L5/E5 band have a chipping rate ten times higher than the signals in the L1/E1 band. This is really beneficial in terms of positioning accuracy to counteract the large GDOP present at very high altitudes. However, the cost to pay is an increase in computational burden, and as a higher chipping rate means a higher rate of change of the code Doppler, a more difficult signal acquisition.

In the first step of the project reported in this paper, we are considering the GPS L1 C/A signal because it is currently transmitted by all the GPS satellites, as well as the GPS L5 signal because of the accuracy improvements it brings. In a second and future step, we will also include the processing of the Galileo signals that will bring a significant improvement of the GDOP.

## III. GNSS SIGNALS CHARACTERISTICS

The following analysis is carried out by using our multi-GNSS full constellation simulator (Spirent GSS8000), which can accurately model both the GPS and Galileo constellations, including the GPS L1 and L5, Galileo E1 and E5 signals, and the 3-D transmitter and receiver antenna patterns. In this section, we report the analysis results obtained for the GPS signals, as they are the ones considered in this first project step. A more extended description of our analysis that includes the Galileo signals as well is reported in [7].

### Simulation Models and Assumptions

According to [9], we considered a GPS constellation made of 31 GPS satellites, allocated in the six orbital planes (as described in [10]).

As the GNSS transmitter antennas point to the Earth to primarily serve the Earth's users, this has a significant effect for space vehicles orbiting above the GPS constellation, which very often can only receive the GPS signals from the spillover of the GNSS signals around the Earth mask, and from the transmitting antennas side lobes. To model accurately the 3-D GPS antenna patterns, we used the pattern from Block II-A as defined in [11] and provided by Spirent, for both GPS L1 and GPS L5, as we could not find a more accurate source of information.

In the simulations, the signal strength was modelled to provide realistic signal levels at the receiver position, taking into account the transmitting antenna and the signal propagation losses. For GPS L1 C/A and GPS L5, according to [10], we assumed a power reference level (guaranteed minimum signal level) of –128.5 dBm and –127 dBm, respectively. In addition, we added a global signal strength offset of +3 dB to account for the difference between the guaranteed minimum transmitted signal level and the real one. Indeed, as suggested in [12], the transmitted signal powers are typically from 1 to 5 dB higher than the reference value.

We also assumed that all the GPS satellites transmit both GPS L1 C/A both GPS L5 signals.

### Signal Power and Dynamics

According to [13], it is possible to calculate the carrier-to-noise ratio C/No (in dB-Hz) from the received power $P_r$ (in dBm) by using the following formula, valid for a front-end noise figure of 2 dB using live signals (i.e., for an effective antenna temperature of 130 K):

$$C/_{No} = P_r + 174. \quad (1)$$

Figure 3 shows the minimum sensitivity required to acquire and track at least 1, 2, 3 or 4 GPS L1 C/A signals

simultaneously, as a function of the altitude, during the full considered trajectory, by assuming a 0 dBi receiver antenna gain. The same values are plotted as a function of the time as well in Figure 4. It can be seen that to always track four GPS L1 C/A signals, the minimum sensitivity required is approximately –175 dBm, and tolerating some short outages (5 peaks visible in Figure 3) the minimum is approximately –168 dBm. For the GPS L5 signal, according to its power reference (1.5 dB higher) we have approximately the same trend with an offset of +1.5 dB.

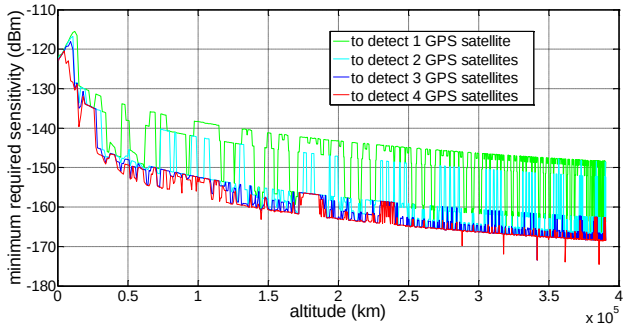


**Figure 3: Minimum sensitivity required to acquire and track 1, 2, 3, 4 L1 C/A GPS signals simultaneously for each altitude of the defined trajectory, assuming a 0 dBi receiver antenna gain.**

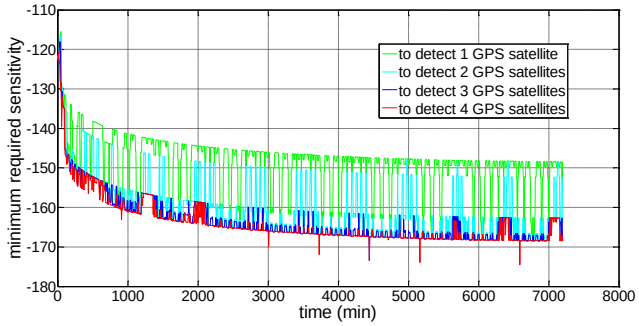


**Figure 4: Minimum sensitivity required to acquire and track 1, 2, 3, 4 L1 C/A GPS signals simultaneously over the time of the defined trajectory, assuming a 0 dBi receiver antenna gain.**

Figure 5 and Figure 6 illustrate respectively all the possible combinations of Doppler shift-received power and all the possible combinations of Doppler rate-received power, by considering all the GPS satellites during the full considered trajectory and by assuming a 0 dBi receiver antenna gain. As expected, the highest dynamics (doppler shift up to 50 kHz and doppler rate up to -65 Hz/s) are concentrated in the first portion of the trajectory (in LEO), corresponding to the highest power levels received where the receiver is below the GPS constellation. As soon as the receiver is far from the Earth (power received below –150 dBm), the Doppler is between –30 and 20 kHz, and the Doppler rate is within ± 5 Hz/s.

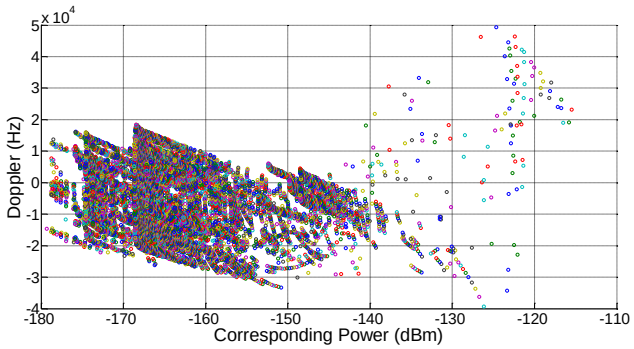


**Figure 5: Possible combinations of Doppler shift and power levels during the whole considered trajectory, assuming a 0 dBi receiver antenna gain.**

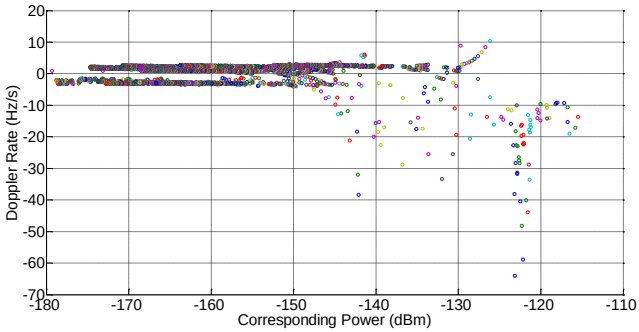


**Figure 6: Possible combinations of Doppler rate and power levels during the whole considered trajectory, assuming a 0 dBi receiver antenna gain.**

## Geometry Error Factor

Figure 7 shows the GDOP according to the altitude for the defined trajectory. The values in blue are calculated by considering only the four GPS satellites from which the received signal power is the strongest, while the values in green are calculated for all the line of sight (LOS) GPS satellites. As expected, by considering the very large distance between the GPS satellites and the receiver when it is close to the Moon, the GDOP becomes huge. In fact, although the final GNSS positioning accuracy is determined by several parameters, the GDOP can be considered as the highest positioning error contribution in very high Earth orbit. This is mainly due to the very limited region in the field of view where the GPS satellites can be seen. Fortunately, as already mentioned in Section II, the use of a second constellation such as Galileo can reduce this GDOP error factor by over a factor of two (see [5], [7]).

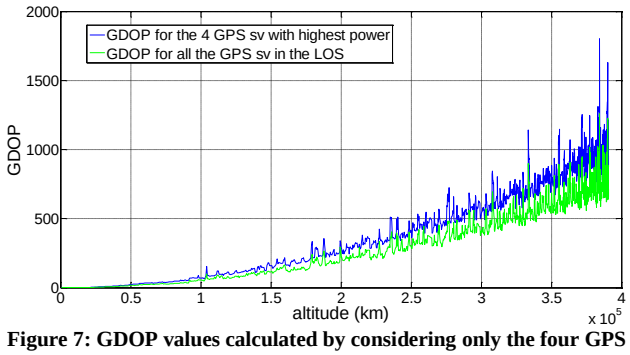


**Figure 7: GDOP values calculated by considering only the four GPS satellites with highest power (in blue), and GDOP values calculated for all the GPS satellites in the LOS, for each altitude of the defined trajectory.**

## IV. OVERALL ARCHITECTURE OF THE SYSTEM

In the designed architecture shown in Figure 8, an Inertial Measurement Unit (IMU) provides position $\boldsymbol{r}_{INS}$, velocity $\boldsymbol{v}_{INS}$ and attitude $\boldsymbol{R}_{INS}$ through the mechanization of their measurements, with high output rate (flow line in yellow), equal to or higher than 50 Hz. A Star Tracker measures accurately the attitude $\boldsymbol{R}_{ST}$ with lower rate and calibrates periodically (flow line in green) the higher rate INS attitude estimation (provided by the gyros), otherwise affected by drift and angular random walk. The inertial navigation solution calibrated by the Star Tracker ($\boldsymbol{r}_{INS}, \boldsymbol{v}_{INS}, \boldsymbol{R}_{ST}$) is then integrated via an Extended Kalman Filter (EKF) to the lower rate (equal to or lower than 5 Hz) GPS measurements of pseudorange $\rho$, pseudorange rate $\dot{\rho}$, position $\boldsymbol{r}_{GPS,sv}$ and velocity $\boldsymbol{v}_{GPS,sv}$ of the GPS satellites (outputted by the GPS satellites kinematics calculation from ephemeris and transmit time). The GPS/INS integration rate corresponds to the GPS output rate (lower than for the INS). The GPS/INS integration output includes the integrated navigation solution and some corrections (i.e. receiver clock bias and receiver clock drift) that are fed back to the GPS receiver. Then the integrated navigation solution is filtered by an orbital forces model through an orbital filter. Hence, every time it is available, the integrated filtered navigation solution is used as feedback to reinitialize and then calibrate the inertial navigation propagation, else affected by unavoidable drifts. The inertial navigation solution, periodically calibrated, is used as GPS aiding.

When the non-gravitational forces are smaller than the accuracy of the accelerometers (that measure the proper acceleration, which does not include gravitational accelerations), then the translational part of the inertial navigation solution, being corrected by the orbital filter, corresponds to the position and velocity estimates provided by the orbital filter itself. However, the accelerometers can measure the proper acceleration of the space vehicle during translational maneuvers. The corrected inertial solution provides a precious aiding to the GPS receiver. By estimating receiver clock bias and drift, expected signal frequency and list of visible GPS satellites; it allows the receiver to tolerate higher dynamics, by reducing the correlation search space and accordingly, it enables higher integration time for higher sensitivity in acquisition and tracking. In fact, as mentioned in [14], an a-priori knowledge of position and velocity limits the number of cells that need to be searched to acquire the signal and in reacquisition, where the GNSS satellite positions and velocities are already estimated and the receiver clock offset is calibrated, the number of cells to search can be reduced significantly, allowing very long dwell times in each cell. When the tracking loops are assisted by an inertial navigation solution, they only need to track the receiver clock noise and the error in the inertial solution, rather than the absolute dynamics at the user antenna. This enables to use narrower tracking loop bandwidths, improving noise resistance and allowing tracking at a lower C/N0 (see, e.g., [14], [15]). Finally, the inertial position and velocity solution is initialized by the standalone GPS solution, while the inertial attitude solution is initialized by the standalone Star Tracker solution.

Such architecture is designed to provide a continuous and complete navigation solution (position, velocity and attitude) as output of a single unit. The aviation grade INS considered brings a direct improvement in the navigation performance since it reduces the standard deviation of the GNSS error, it allows high output rate, high low-term accuracy in high dynamics of LEO and it ensures a solution when the number of available GNSS satellites is lower than four. On the other hand, the use of GNSS receiver and Star Tracker absolute measurements, although with lower output rate, stops the inertial error accumulation, drawback of the dead reckoning systems.

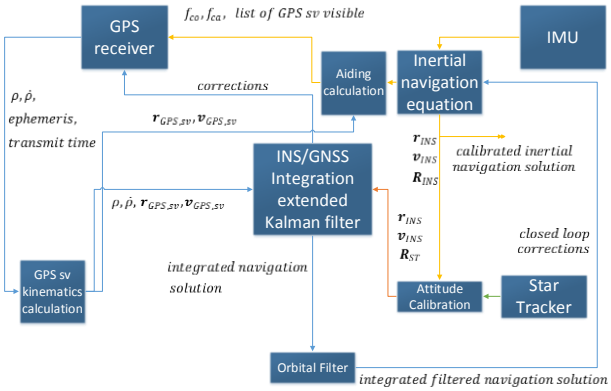


**Figure 8: Block scheme of the GNSS/INS/Star Tracker integrated system overall architecture.**

## V. GPS ACQUISITION

### Acquisition Strategy

The structure of acquisition is illustrated in Figure 9. It is based on the parallel code search (PCS) that use fast Fourier transform (FFT) to compute the correlation [16].

In order to make a balance between performance and required resources, the full bit method (that means 20 ms

coherent integration time for GPS L1 C/A) described in [17] with ten branches is chosen to handle the data bit transition problem. In addition, in order to achieve higher sensitivity, we also considered increasing the whole integration time with non-coherent integrations.
The parameters of the front-end used in our implementation are summarized in Table 2.

**Table 2: Parameters of the front-end.**

| Quantity (unit) | Value |
|---|---|
| Noise figure of the front-end (dB) | 2 |
| Sampling frequency (MHz) | 40.96 |
| Analog IF (MHz) | 53.78 |
| Digital IF (MHz) | 12.82 |
| Resolution (bit) | 4 |
| Output format | real |

In order to decrease the computation burden, a down-sampling process is needed. After down-sampling, the sampling frequency is 4.096 MHz, and the resolution is 8 bits both for I and Q.
In order to define a power threshold, we have considered a 10 dBi gain receiver antenna. Indeed, it is reasonable to assume that the host space vehicle will be equipped by more than one receiver antenna (placed on different faces of the vehicle) and/or that at least one antenna points in the GPS satellites direction in order to provide 10 dB gain during the whole trajectory, also over the GPS constellation (at very high altitudes, it corresponds to an Earth-pointing space vehicle approximately). From Figure 3 and Figure 4, we have seen that the minimum sensitivity to acquire 4 satellites is approximately –168 dBm, thus, by considering a receiver antenna gain of 10 dBi, in order to dectect 4 satellites or more, we take into consideration –159 dBm as a slightly higher sensitivity value than the minimum required.
The front-end noise figure of our implementation is 2 dB, which means that, by using Eq. (1), –159 dBm corresponds to an IF C/N0 of 15 dB-Hz [13].

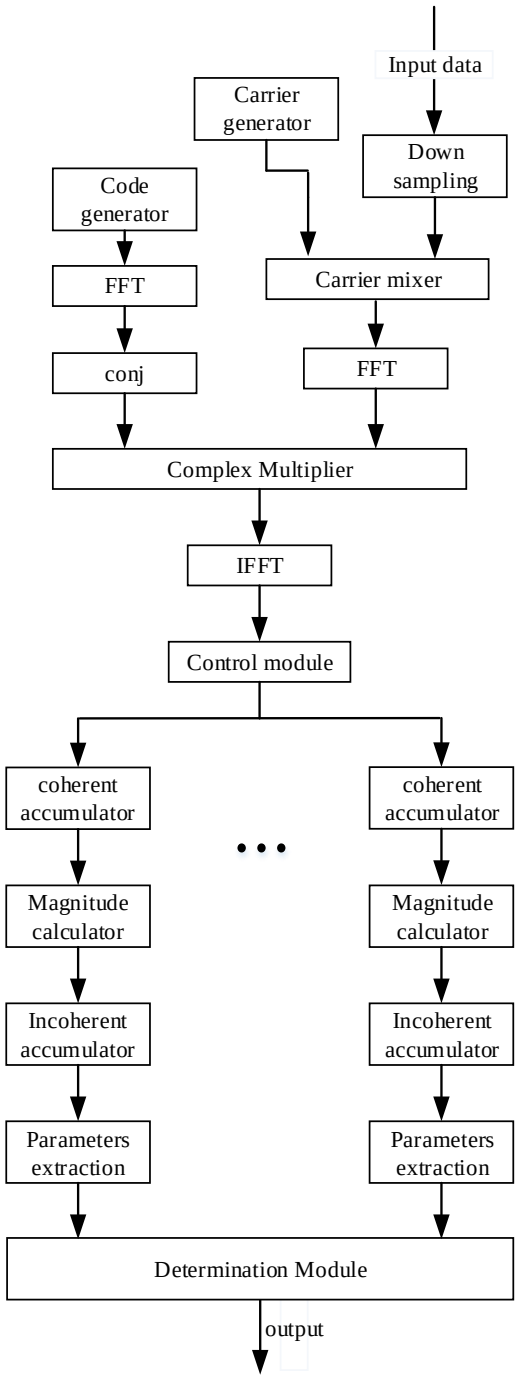


**Figure 9: Block scheme of the acquisition structure.**

In order to estimate the total required integration time for the above sensitivity levels, we conducted a theoretical analysis according to the method discussed in [13]. The results are presented in Table 3 and Table 4 for both the worst and the average cases (in terms of frequency mismatch loss, code alignment loss and data bit alignment loss).

**Table 3: Theoretical analysis of the worst case.**

| Quantity (unit) | Value |
|---|---|
| Sensitivity (dBm) | –159 |
| IF C/N0 (dB-Hz) | 15 |
| Coherent gain (dB) | 46 |
| Quantization loss (dB) | 0.05 |
| Frequency mismatch loss (dB) | 0.912 |
| Code alignment loss (dB) | 1.1586 |
| Data bit alignment loss (dB) | 0.9151 |
| Squaring loss (dB) | 5.7373 |
| Final SNR (dB) | 16 |
| Non-coherent gain needed (dB) | 26.767 |
| Number of non-coherent integration | 475 |
| Total integration time (s) | 9.5 |
| Maximum Tolerable Doppler rate (Hz/s) | 2.631 |
| Frequency search step (Hz) | 25 |
| Code search step (chip) | 0.25 |

**Table 4: Theoretical analysis of the average case.**

| Quantity (unit) | Value |
|---|---|
| Sensitivity (dBm) | –159 |
| IF C/N0 (dB-Hz) | 15 |
| Coherent gain (dB) | 46 |
| Quantization loss (dB) | 0.05 |
| Frequency mismatch loss (dB) | 0.2972 |
| Code alignment loss (dB) | 0.56 |
| Data bit alignment loss (dB) | 0.4455 |
| Squaring loss (dB) | 4.2 |
| Final SNR (dB) | 16 |
| Non-coherent gain needed (dB) | 23.54 |
| Number of non-coherent integration | 226 |
| Total integration time (s) | 4.52 |
| Maximum Tolerable Doppler rate (Hz/s) | 5.53 |
| Frequency search step (Hz) | 25 |
| Code search step (chip) | 0.25 |

The maximum integration time is restricted by the FPGA platform, since there is a large amount of data needed to be saved. In our project, an Altera Stratix III FPGA (EP3SE260F1152) is used. The input data is saved in an external DDR2 SDRAM and the maximum data that can be saved in this platform is 15.6 s ($1.024 \times \frac{10^9}{16} / (4.096 \times 10^6)$), where $1.024 \times 10^9$ is the volume of the DDR2 SDRAM in bits, 16 is the total length of I and Q which is mentioned before, $4.096 \times 10^6$ is the sampling rate.

Therefore, the memory in our FPGA platform is sufficient to acquire GPS L1 C/A signals down to -159 dBm also in the worst case conditions of Table 4.

From Figure 5, in most of the considered space trajectory, the frequency search space is ±25 kHz. Because of such large frequency search space and of the required very high sensitivity, the acquisition time would be very long, unless an acquisition aiding is used. In fact, without any aiding or assistance, the acquisition time would be

$$T_A = T_I + N_{FB} T_{FB}, \qquad (2)$$

where $T_I$ is the time required for saving the data (in this case 9.5 s), $N_{FB}$ is the number of frequency bins to be searched (in this case 2000 = 50k / 25) and $T_{FB}$ is the time needed to search 1 frequency bin, which is defined as:

$$T_{FB} = \frac{f_{S,L1} T_I}{f_{FPGA}} = \frac{4.096\ 10^6 \times 9.5}{163.84\ 10^6} \approx 237.5 \text{ ms}, \qquad (3)$$

where $f_{S,L1}$ is the sampling rate of L1 after down sampling, $T_I$ is the total integration time, and $f_{FPGA}$ is the processing frequency of the FPGA. Hence, the whole acquisition time needed without external aiding would be 484.5 s ($9.5 + 2000 \times 0.2375$).

**Acquisition Aiding**

With the aiding of INS, Star Tracker and orbital filter, the frequency search space can be much smaller, depending mainly on the Doppler aiding accuracy and on the residual Doppler still present due to the finite accuracy of the local oscillator frequency. E.g., in [18] a Doppler aiding of 0.05 Hz provided by an orbital filter has been obtained for Low Lunar orbit (LLO). Moreover, assuming an OCXO with a typical accuracy of $2 \cdot 10^{-8}$ [19], the clock frequency uncertainty will be $\pm 31.55$ Hz. By using these values in Eq. (2) the acquisition time can be decreased tremendously to 10.21 s $\left(9.5 + ceil\left(2 \times \frac{31.55}{25}\right) \times 0.2375\right)$. Furthermore when the receiver clock offset and drift are estimated by the navigation filter (as described in Section VII), the frequency search space will be very close to the frequency uncertainty only due to the frequency aiding and then the acquisition time will be even smaller.

Besides decreasing the acquisition time for one PRN, the supportive systems aiding can also be used to decrease the number of PRNs to be searched, assuming knowledge of the GNSS almanacs (which can be downloaded from several satellites being tracked during the mission).

## VI. GPS TRACKING

**Tracking Strategy**

In this project, an EKF based carrier tracking structure is used to achieve the high sensitivity. The new carrier tracking structure is implemented for each satellite tracking channel, replacing the traditional carrier phase discriminator and loop filter. The EKF uses a dynamical and statistical model of the system to estimate and correct the parameters of the signals. The estimation is optimized in the mean square error (MSE) sense for Gaussian input signals. Unlike the conventional tracking loop, the changing of the environment noise is taken into account and the parameters of the tracking structure are corrected over time. This property makes the EKF tracking loop able to work in very noisy contexts [20]. Because of the strong extensibility of EKF, this tracking structure can be linked to supportive systems or other subsystems easily.

Signal Model

After the acquisition process, a rough estimation of the carrier frequency and code phase is obtained. Through these rough parameters, the receiver accumulates correlations between the received low intermediate frequency (IF) signal and the replica signal. After correlation and accumulation, assuming that the data bit edge is well matched, the correlation value can be expressed as [20]:

$$corr(n) = \frac{A_{(n)} d_{(n)} R_{(n)} \sin(\pi f_{D(n)} T_{coh})}{\pi f_{D(n)} T_{coh}} e^{j\left[2\pi f_{D(n)}\left(\frac{T_{coh}}{2}\right)+\theta_{(n)}\right]} + N_{i(n)} + jN_{q(n)}, \quad (4)$$

where $A_{(n)}$ is the amplitude of the signal, $d_{(n)}$ is the modulated message, $f_{D(n)}$ is the carrier frequency error of the signal, $\theta_{(n)}$ is the carrier phase error, $R_{(n)}$ is the code correlation function, which represent the code phase misalignment loss, $T_{coh}$ is the coherent integration time, which is 20 ms, corresponding to one bit of the GPS navigation message, and $N_{i(n)}$ and $N_{q(n)}$ are the complex thermal noise terms.

The goal of the EKF carrier tracking block is to estimate three parameters in (4), namely $A_{(n)}$, $f_{D(n)}$ and $\theta_{(n)}$. In order to make this structure satisfying the high dynamic context, $f_{D(n)}$ is divided into two part, and can be expressed as:

$$f_{D(n)} = f_{bD(n)} + a_{(n)} T_s, \quad (5)$$

where $T_s$ represents the time interval between two successive correlation values (in this design it is equivalent to $T_{coh}$), $a_{(n)}$ represents the Doppler rate of the signal, and $f_{bD(n)}$ the initial Doppler shift at time $n$.

System dynamic model

The corresponding system dynamic model is defined as:

$$\boldsymbol{X}_{(n+1)} = \boldsymbol{F}\boldsymbol{X}_{(n)} + \boldsymbol{W}_{(n)}, \quad (6)$$

where $\boldsymbol{X}_{(n)}=[\theta_{(n)}, f_{bD(n)}, a_{(n)}, A_{(n)}]^T$, and

$$\boldsymbol{F} = \begin{bmatrix} 1 & T_s & {T_s}^2/2 & 0 \\ 0 & 1 & T_s & 0 \\ 0 & 0 & 1 & 0 \\ 0 & 0 & 0 & 1 \end{bmatrix}, \quad (7)$$

$\boldsymbol{X}_{(n)}$ represents the state vector of the tracking loop at time step $n$, $\boldsymbol{F}$ is a constant propagation matrix of state vector and $\boldsymbol{W}$ is the noise of state vector. By tuning the matrix $\boldsymbol{F}$, the performance of the tracking loop can be improved.

Measurement model

If the standalone GNSS receiver is considered only, the measurement model is described as:

$$\boldsymbol{Z}_{standalone\,(n)} = \boldsymbol{h}_{standalone}(\boldsymbol{X}_{(n)}) + \boldsymbol{V}_{standalone} = \begin{bmatrix} corrI_{(n)} \\ corrQ_{(n)} \end{bmatrix} + \begin{bmatrix} N_{i(n)} \\ N_{q(n)} \end{bmatrix} = \begin{bmatrix} A_{(n)}\cos(\Theta_{(n)}) \\ A_{(n)}\sin(\Theta_{(n)}) \end{bmatrix} + \begin{bmatrix} N_{i(n)} \\ N_{q(n)} \end{bmatrix}, \quad (8)$$

where $\boldsymbol{h}_{standalone}(\boldsymbol{X}_{(n)})$ is the measurement equation, $\boldsymbol{V}_{standalone}$ represents the observation noise, induced by the thermal noise, where $corrI_{(n)}$ and $corrQ_{(n)}$ represent the in-phase and quadrature correlation values, which correspond to the first term on the right side of Eq. (4), and $\Theta_{(n)}$ is the total carrier phase, which depends on the state vector $\boldsymbol{X}_{(n)}$. Since the relationship between the measurement and the state is not linear, in the iteration procedure the measurement is linearized to be represented by the measurement matrix $\boldsymbol{H}$, which is the Jacobian matrix of $\boldsymbol{h}_{standalone}$.

**Tracking Aiding**

When the assistance from navigation module is taken into consideration, the measurement model can be described as

$$\begin{aligned} \boldsymbol{Z}_{GNSS-aid\,(n)} &= \boldsymbol{h}_{GNSS-aid}(\boldsymbol{X}_{(n)}) + \boldsymbol{V}_{GNSS-aid} \\ &= \begin{bmatrix} corrI_{(n)} \\ corrQ_{(n)} \\ f_{assistance(n)} \end{bmatrix} + \begin{bmatrix} N_{i(n)} \\ N_{q(n)} \\ N_{NAV(n)} \end{bmatrix} \\ &= \begin{bmatrix} \cos(\Theta_{(n)}) \\ \sin(\Theta_{(n)}) \\ f_{est(n)} + f_{clock_{error}} \end{bmatrix} + \begin{bmatrix} N_{i(n)} \\ N_{q(n)} \\ N_{NAV(n)} \end{bmatrix} \end{aligned} \quad (8)$$

where $f_{assistance(n)}$ is the assistance frequency that contains two parts: $f_{est(n)}$ is the assistance frequency estimated by the supportive systems solution and $f_{clock\_error}$ is the inverse of the estimated receiver clock error. $N_{NAV}$ is the observation noise of the supportive systems.

According to the above equation and the standard EKF estimation procedure, the EKF-based carrier tracking structure can be realized as depicted in Figure 10. The initial value of the iteration is the acquired frequency.

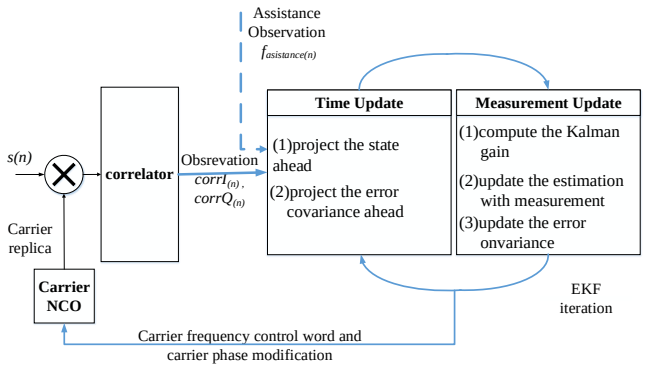


**Figure 10: Block diagram of EKF based carrier tracking structure.**

For the purpose of minimizing the computational burden of the tracking module, the code tracking loop is realized in traditional carrier aided DLL with 0.5 Hz noise bandwidth.

## VII. GPS/INS/STAR TRACKER NAVIGATION

### Integrated Navigation Solution

As the current aim of our project is to build a proof of concept demonstrator for the considered lunar mission, we did not develop any specific IMU or Star Tracker. These two subsystems have been modelled in Matlab in order to test the whole multi-sensor integrated navigation system in post-processing mode on a computer (in a second step, the navigation algorithm will be tested in real time with the receiver signal processing FPGA-based hardware).

Aviation grade INS has been selected for initially as a reasonable compromise between performance, dimensions and cost.

Table 5 reports the specifications of the modelled IMU subsystem, according to the values proposed in reference [14].

A Star Tracker is an optical device that measures the positions of stars using photocells or a camera [21] and from such observations it estimates the attitude. For our study, we have considered the "Blue Canyon Technologies Nano-Star Tracker", a precise 3-axis stellar attitude determination in a micro-package, which allows high performance attitude determination for very small satellites like CubeSats. With a nominal power consumption equal or lower than 0.5 W and a very small volume of 10 × 6.73 × 5 $cm^3$ (with baffle) [22], such attitude sensor can reasonably be integrated with an IMU and a GNSS receiver in one single small unit. The attitude estimation of this sensor has been modelled in Matlab by considering its datasheet [22], in particular a bore-sight accuracy of 6″ and a roll axis accuracy of 40″.

By using the Star Tracker in conjunction with a precise time reference (provided by the GNSS receiver) and the IMU device consisting of gyroscopes and accelerometers (inertial navigator), the on board processor can correct many of the inertial navigator errors, in particular the inertial navigator's gyroscopes errors that result in attitude drift.

**Table 5: IMU specifications according to the values proposed in reference [14].**

| Quantity (unit) | Values |
|---|---|
| Accelerometer biases x,y,z ($\mu g$) | $[30 \quad -45 \quad 26]$ |
| Gyro biases (°/h) | $[-0.0009 \quad 0.0013 \quad -0.0008]$ |
| Accelerometer scale factor and cross coupling errors (ppm) | $\begin{bmatrix} 100 & -120 & 80 \\ -60 & -120 & 100 \\ -100 & 40 & 90 \end{bmatrix}$ |
| Gyro scale factor and cross coupling errors (ppm) | $\begin{bmatrix} 8 & -120 & 100 \\ 0 & -6 & -60 \\ 0 & 0 & -7 \end{bmatrix}$ |
| Accelerometer noise root PSD $(\mu g/\sqrt{\text{Hz}})$ | 20 |
| Gyro noise root PSD $(°/\sqrt{\text{h}})$ | 0.002 |
| Accelerometer quantization level $(\text{m/s}^2)$ | $5 \cdot 10^{-5}$ |
| Gyro quantization level (rad/s) | $1 \cdot 10^{-6}$ |

As suggested in [14], pseudorange and pseudorange rate measurements from the GNSS receiver, position and velocity of the corresponding GNSS satellites from ephemeris and transmit time, and the inertial navigation solution from the IMU are inputted in the EKF to correct the inertial navigation solution. In particular, the inertial navigation solution, together with the GNSS satellites positions and velocities is used to predict the GNSS pseudorange and pseudorange rate measurements. Hence, in one complete cycle, the EKF corrects the inertial navigation solution and updates the estimates of the IMU biases, GNSS receiver clock offset and bias and state error covariance matrix as well. The navigation integration is thus performed in the range domain with the GNSS receiver output rate. Simultaneously, the inertial solution, although corrected only when the EKF output is updated, is available with higher rate and high accuracy (within one EKF cycle) and then used to predict the signals frequency as aiding in tracking and acquisition. According to [14], range-domain integration with inertial aiding of the GNSS tracking loops is described as "Ultra Tightly Coupled (UTC) GNSS/INS integration".

The continuous time system model and the measurement model are respectively represented by:

$$\dot{\boldsymbol{x}}(t) = \boldsymbol{f}\big(\boldsymbol{x}(t)\big) + \boldsymbol{G}(t)\boldsymbol{w_s}(t), \qquad (9)$$

and

$$\boldsymbol{z}(t) = \boldsymbol{h}\big(\boldsymbol{x}(t)\big) + \boldsymbol{w_m}(t), \qquad (10)$$

where:

$\boldsymbol{x}(t)$ is the state vector,
$\boldsymbol{f}(\boldsymbol{x}(t))$ is a nonlinear function of the state vector,

| | |
|---|---|
| $\boldsymbol{G}(t)$ | is the system noise distribution matrix, |
| $\boldsymbol{w_s}(t)$ | is the system noise vector, |
| $\boldsymbol{z}(t)$ | is the measurement vector, |
| $\boldsymbol{h}(\boldsymbol{x}(t))$ | is a nonlinear function of the state vector |
| $\boldsymbol{w_m}(t)$ | is the measurement noise vector. |

Table 6 shows the Kalman filter algorithm [14], where:

| | |
|---|---|
| $\hat{\boldsymbol{x}}_k^-$ | is the a priori state estimate at a time step $k$, |
| $\hat{\boldsymbol{x}}_{k-1}^+$ | is the a posteriori state estimate at a time step $k$-1, |
| $\boldsymbol{\Phi}_{k-1}$ | is the state transition matrix at a time step $k$-1, |
| $\boldsymbol{P}_k^-$ | a priori estimate error covariance at a time step $k$, |
| $\boldsymbol{P}_{k-1}^+$ | a posteriori estimate error covariance at a time step $k$-1, |
| $\boldsymbol{Q}_{k-1}$ | is the discrete process noise covariance a time step $k$-1, |
| $\boldsymbol{R}_k$ | is the discrete measurement noise covariance at a time step $k$, |
| $\boldsymbol{H}_k$ | is the measurement matrix at a time step $k$, |
| $\boldsymbol{K}_k$ | is the Kalman gain at a time step $k$, |
| $\boldsymbol{z}_k$ | is the measurement vector at a time step $k$, |
| $\delta\mathbf{z}_k^-$ | is the innovation measurement vector at a time step $k$, |
| $\boldsymbol{I}$ | is a unit matrix. |

**Table 6: Kalman filter algorihm for the navigation.**

| Quantity | Formulation |
|---|---|
| Predicted state vector | $\hat{\boldsymbol{x}}_k^- = \boldsymbol{\Phi}_{k-1}\hat{\boldsymbol{x}}_{k-1}^+$ |
| Predicted system noise covariance matrix | $\boldsymbol{P}_k^- = \boldsymbol{\Phi}_{k-1}\boldsymbol{P}_{k-1}^+\boldsymbol{\Phi}_{k-1}^T + \boldsymbol{Q}_{k-1}$ |
| Kalman Gain matrix | $\boldsymbol{K}_k = \boldsymbol{P}_k^-\boldsymbol{H}_k^T(\boldsymbol{H}_k\boldsymbol{P}_k^-\boldsymbol{H}_k^T + \boldsymbol{R}_k)^{-1}$ |
| Corrected state estimate | $\hat{\boldsymbol{x}}_k^+ = \hat{\boldsymbol{x}}_k^- + \boldsymbol{K}_k(\boldsymbol{z}_k - \boldsymbol{H}_k\hat{\boldsymbol{x}}_k^-) = \hat{\boldsymbol{x}}_k^- + \boldsymbol{K}_k\delta\boldsymbol{z}_k^-$ |
| Corrected system noise covariance matrix ( normal form) | $\boldsymbol{P}_k^+ = (\boldsymbol{I} - \boldsymbol{K}_k\boldsymbol{H}_k)\boldsymbol{P}_k^-$ |
| Corrected system noise covariance matrix ( Joseph form) | $\boldsymbol{P}_k^+ = (\boldsymbol{I} - \boldsymbol{K}_k\boldsymbol{H}_k)\boldsymbol{P}_k^-(\boldsymbol{I} - \boldsymbol{K}_k\boldsymbol{H}_k)^T + \boldsymbol{K}_k\boldsymbol{R}_k\boldsymbol{K}_k^T$ |

The transition matrix can be expressed as:

$$\boldsymbol{\Phi}_{k-1} = exp(\boldsymbol{F}_{k-1}\tau_s) \cong (I + \boldsymbol{F}_{k-1}\tau_s), \qquad (11)$$

while for the EKF:

$$\boldsymbol{F}_{k-1} = \frac{\partial f(x)}{\partial \boldsymbol{x}}\Big|_{\boldsymbol{x}=\hat{\boldsymbol{x}}_{k-1}^+} \text{ and } \boldsymbol{H}_k = \frac{\partial \boldsymbol{h}(x)}{\partial \boldsymbol{x}}\Big|_{\boldsymbol{x}=\hat{\boldsymbol{x}}_k^-} = \frac{\partial \boldsymbol{z}(x)}{\partial \boldsymbol{x}}\Big|_{\boldsymbol{x}=\hat{\boldsymbol{x}}_k^-}. \qquad (12)$$

In this case the state vector is $\boldsymbol{x} = \begin{bmatrix} \delta\boldsymbol{\varphi} \\ \delta\boldsymbol{v} \\ \delta\boldsymbol{r} \\ \boldsymbol{b}_a \\ \boldsymbol{b}_g \\ \delta\rho_c^{GPS} \\ \delta\dot{\rho}_c^{GPS} \end{bmatrix}$,

where:

| | |
|---|---|
| $\delta\boldsymbol{\varphi}$ | is the attitude error, |
| $\delta\boldsymbol{v}$ | is the velocity error, |
| $\delta\boldsymbol{r}$ | is the position error, |
| $\boldsymbol{b}_a$ | are the accelerometer biases, |
| $\boldsymbol{b}_g$ | are the gyros biases, |
| $\delta\rho_c^{GPS}$ | is the receiver clock offset, |
| $\delta\dot{\rho}_c^{GPS}$ | is the receiver clock drift. |

The measurement vector is $\boldsymbol{z} = \begin{bmatrix} \boldsymbol{\rho}_{GPS} \\ \dot{\boldsymbol{\rho}}_{GPS} \end{bmatrix}$, where:

| | |
|---|---|
| $\boldsymbol{\rho}_{GPS}$ | are the pseudoranges of the available GPS satellites, |
| $\dot{\boldsymbol{\rho}}_{GPS}$ | are the pseudorange rates of the available GPS satellites. |

The measurement innovation vector includes the differences between the GPS measured pseudorange and pseudorange rates and the corresponding values predicted by the corrected inertial navigation solution at the same time of validity, by using estimated receiver clock offset and drift, and navigation data-indicated satellite positions and velocities.
The matrices $\boldsymbol{\Phi}_{k-1}$, $\boldsymbol{Q}_{k-1}$, $\boldsymbol{R}_k$,$\boldsymbol{H}_k$ have been implemented according to [14].

**Integration to the Orbital Forces Model**

Vehicles in space may have unknown, quasi-constant orbit parameters, but their trajectories over the short-term are essentially defined by a finite set of parameters (the orbital parameters). GNSS vehicle tracking in fact, well described in [23], corresponds to an orbit determination problem. The orbital parameters will change during the orbits like the one here considered, but the problem remains an orbit determination problem with increased uncertainty in initial conditions [23]. Orbit determination consists essentially of a set of mathematical propagation techniques for predicting the future positions of orbiting objects (such as moons, planets, and spacecraft) from different kind of observations. As time progresses, because of the inevitable errors of modelling the orbital perturbations, the actual

path of an orbiting object tends to diverge from the predicted path and a new orbit determination using new observations is needed to re-calibrate knowledge of the orbit. In our problem, the observations are the GNSS/INS/Star Tracker integrated solutions. An additional non-linear Kalman filter predicts the observations by propagating them through an orbital forces model (process of the filter) and fuses it with the observations themselves.

In our case, the optimum Kalman filter tuning might vary with time. In particular, by assuming a dual frequency receiver, the main contribution in the pseudorange measurement noise is the code tracking error, which increases when the C/N0 decreases and then, once over the GPS constellation, when the altitude increases as well. Furthermore, the GPS position accuracy is proportional to GPS satellites geometry factor as well, which also increases with the altitude, as shown in Figure 7. The high changes of standard deviation of GDOP and tracking error along the altitude clearly demonstrate that the measurement noise covariance $\boldsymbol{R}_k$ has to be updated along the altitude in order to keep the filter well-tuned. For these reasons, we are developing an adaptive Kalman filter that estimates the measurement noise covariance $\boldsymbol{R}_k$ as function of the pseudorange measurement noise and GDOP.

## VIII. PRELIMINARY RESULTS

### Acquisition Performance

Figure 11 provides an example of unaided weak GPS L1 C/A acquisition down to –159 dBm (or 15 dB-Hz), obtained by using the strategy described in Section 0 and implemented in our FPGA.

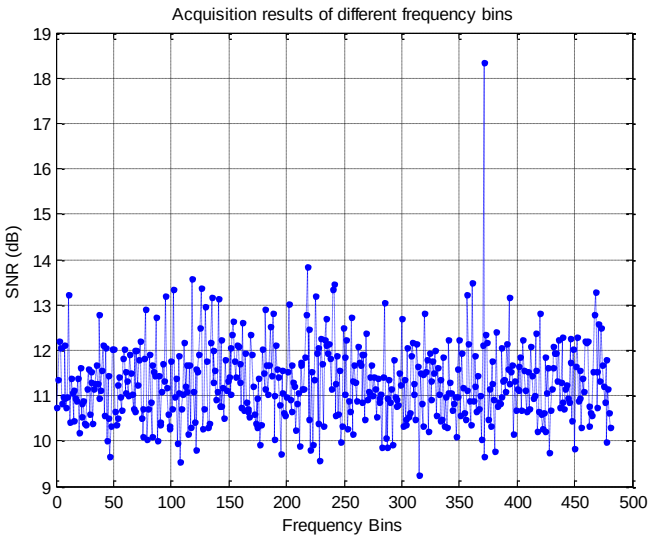


**Figure 11: Example of unaided weak GPS L1 C/A acquisition down to 15 dB-Hz, obtained by using the strategy described in Section 0.**

It can be seen as compared to the other frequency bins, the correct one has the biggest SNR.

### Tracking Performance

Figure 12 represents an example of tracking result comparison between the designed EKF tracking loop and a traditional third order PLL such as discussed in [12]. It is clear that the tracking error of EKF loop is much smaller than the one of the PLL.

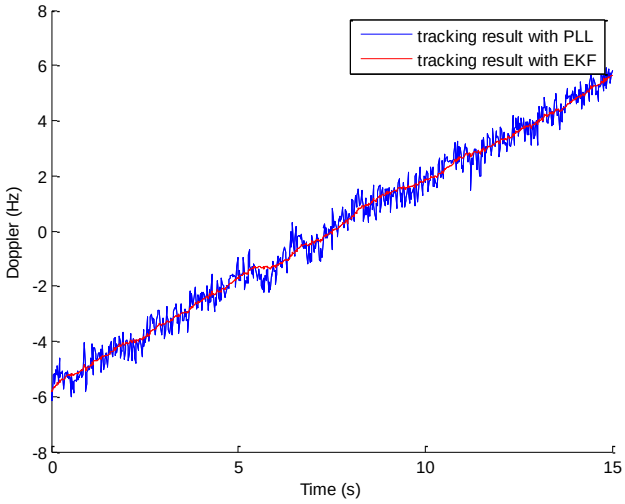


**Figure 12: Tracking results (Doppler offset is removed) comparison between EKF and PLL for a C/N0 of 30 dB-Hz.**

At current time, the proposed tracking structure has been tested by MATLAB simulations, using attenuated GPS signals, for the case of standalone GPS. The simulations have shown that the designed EKF tracking structure provides a GPS L1 C/A sensitivity of –159 dBm (or 15 dB-Hz) by using 20 ms integration time.

### Resultant Availability for GPS L1 C/A

The availability of a signal (or of the GNSS satellite from which it is transmitted) can be defined as a Boolean variable which is true at the time *t* only if:

- the signal transmitter antenna is in the line of sight (LOS) at *t*,
- at *t*, the received signal power is higher than a defined power threshold.

By considering the acquisition and tracking threshold currently achieved of –159 dBm (as described in Sections 0 and VI) and the signal power levels reported in Section III, Figure 13 and Figure 14 respectively show the available GPS satellites over time and the number of simultaneously available GPS satellites for each altitude during the full trajectory defined in Section II.

As shown in Figure 15 and Figure 16, if the power threshold is just 3 dB lower than –159 dBm, after the 3000th min of the orbit the number of available satellites decreases to less than four most of the time, not allowing an absolute position fix for very long time intervals, such as the ones delimited by the two orange rectangles. This

clearly illustrates the need for a minimum -159 dBm sensitivity threshold.

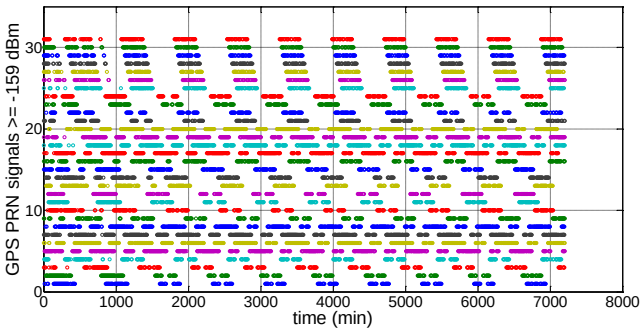


**Figure 13: GPS satellite available for a power threshold of –159 dBm.**

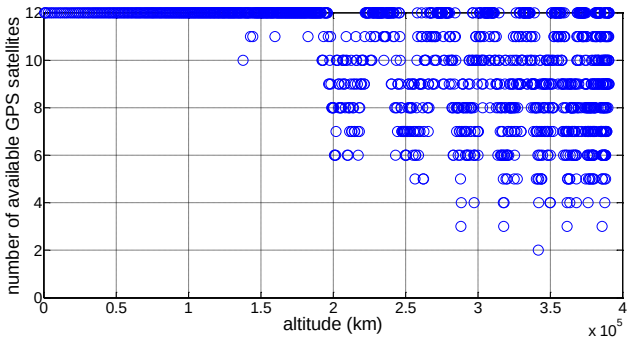


**Figure 14: Number of available GPS satellites for the achieved power threshold of –159 dBm, for each altitude of the defined trajectory.**

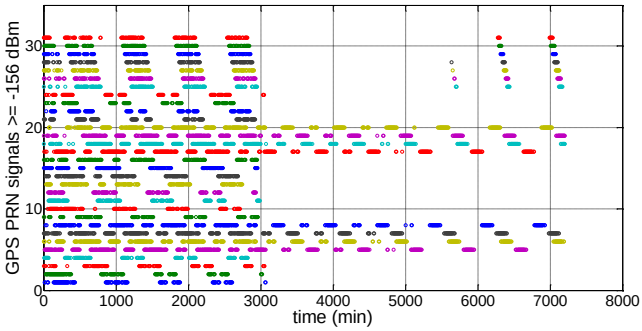


**Figure 15: GPS satellite available for a power threshold of –156 dBm.**

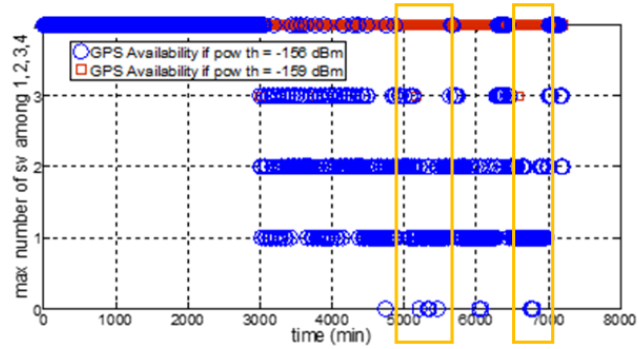


**Figure 16: Maximum number of GPS satellites available, between 1 and 4, for a power threshold of –156 dBm (in blue) and of –159 dBm (in red), over time.**

## Navigation Performance

In order to validate the algorithm proposed in Section VII, and assess the expected performance improvements achievable by integrating the GPS receiver and INS in the pseudo-range domain, several tests have been performed. Figure 17 shows the 3-D position error when the receiver is travelling in the defined trajectory during the first 2900 s (from the perigee at 600 km to approximately the 13 500 km altitude), for the case of a standalone dual frequency (L1 C/A – L5) GPS and for the case of a dual frequency GPS/INS/Star Tracker integration. Such simulation results do not include the beneficial effects of the orbital filter, which is currently still under development.

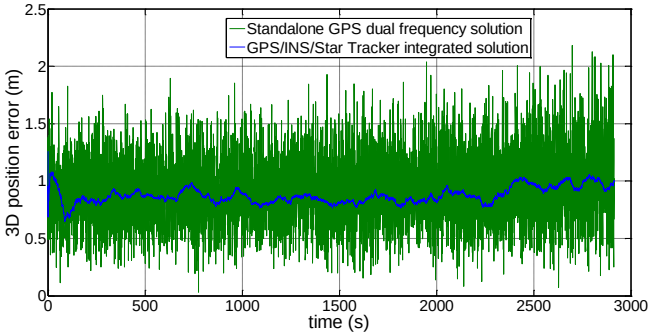


**Figure 17: 3-D position error when the receiver is travelling in the defined trajectory during the first 2900 s for the case of standalone dual frequency L1 C/A – L5 GPS (in green) and for the case of dual frequency GPS/INS/Star Tracker integration (in blue).**

According to [24], the ionosphere signals delays that a space receiver can experience are potentially much larger (more than 150 m) than the delays on signals travelling to a receiver on the Earth (typically 2-30 m). In fact travelling from 600 km upwards, the receiver will almost always be above the ionosphere and therefore signals will only experience delay at negative elevation angles from the Earth horizon, passing through a given altitude of the ionosphere twice. For this reason, as already mentioned in Section II, in our project we foresee the use of a second GPS frequency to remove the potential high ionosphere delay.

If the ionosphere delay is removed by the simultaneous use of two frequencies, according to [12] a considerable contribution in the user equivalent range error (UERE) is the receiver noise, which can be much higher than for terrestrial use due to the much weaker signal power levels. Eq. (13) as suggested in [12] provides the thermal noise range error jitter for BPSK signals.

$$\sigma_{tDLL} = \begin{cases} \sqrt{\frac{B_n}{2C/N_0} D\left(1+\frac{2}{T\,C/N_0(2-D)}\right)}, & D \geq \frac{\pi R_c}{B_{fe}} \\ \sqrt{\frac{B_n}{2C/N_0}\left[\frac{R_c}{B_{fe}}+\frac{B_{fe}T_c}{\pi-1}\left(D-\frac{R_c}{B_{fe}}\right)^2\right]\left(1+\frac{2}{TC/N_0(2-D)}\right)}, & \frac{R_c}{B_{fe}} < D < \frac{\pi R_c}{B_{fe}} \\ \sqrt{\frac{B_n}{2C/N_0}\frac{R_c}{B_{fe}}\left(1+\frac{1}{TC/N_0}\right)}, & D \leq \frac{R_c}{B_{fe}} \end{cases} \quad (13)$$

where $B_{fe} = 26\,\text{MHz}$ is the double sided front-end bandwidth, $R_c = 1.023\,\text{Mchip/s}$ is the chipping rate, $T_c = 1/R_c$ is the chip duration in seconds, $D = 0.1$ chip is the distance between early and late correlators, $B_n = 0.5$ is the loop bandwidth in Hz, and $T = 20\,\text{ms}$ is coherent integration time. Figure 18 illustrates the maximum, median, mean and minimum values of GPS L1 code tracking error $\sigma_{tDLL}$ along the altitude of the considered trajectory, calculated using Eq. (13) and the power of the available signals (the ones that can be acquired and tracked with a threshold of –159 dBm assuming a 10 dBi receiver antenna gain). Since the higher is the altitude the weaker is the signal, as expected, the higher is the code tracking error. Note that the values shown in Figure 18 for GPS L1 C/A have to be divided by factor 10 to be valid for GPS L5, since the L5 chip length is ten times smaller than for L1. Thus, this clearly demonstrates that the use of the second frequency L5 not only is needed to remove most of the pseudorange delay due to the atmosphere, but also to strongly reduce the code tracking error, not negligible in such scenario, most of all by considering that its positioning error effect is amplified by a factor equal to the GDOP, huge at the highest altitudes.

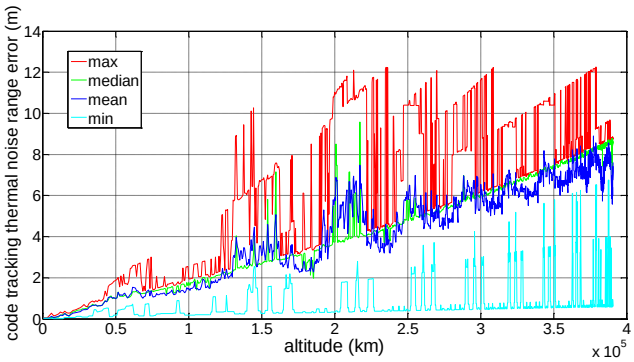


**Figure 18: Theoretical GPS L1 average code tracking error along the altitude of the defined trajectory.**

At very high altitudes up to the Moon, code tracking errors higher than 10 m (due to the very weak signals), ionosphere delays of hundred meters (due to double crossing of the atmosphere), GDOP higher than 1500 (due to the poor GPS satellite geometry) badly limit the use of the single frequency GPS L1 C/A to very poor navigation performance. Thus it certainly demonstrates the need of a more precise GNSS observation (i.e. achievable by using two frequencies and modernized signals or with carrier phase measurement rather than code-phase measurement), and of a larger number of available GNSS satellites (i.e. as a result of using a multi-constellation receiver), as shown in Figure 19 for the combined use of GPS and Galileo constellations.

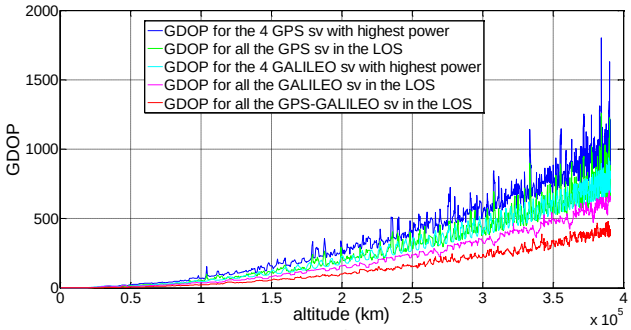


**Figure 19: GDOP values calculated for the GPS, Galileo and GPS-Galileo combined constellations, for each altitude of the considered trajectory.**

## CONCLUSIONS

The proposed multi-sensor navigation system is conceived to acquire and track the weak GNSS signals in HEO up to Moon altitude as well as signals affected by high dynamics in LEO, and to provide not only position and velocity, but also attitude and angular velocity of the vehicle. Consequently, the full kinematic state of the vehicle can be obtained, with high rate, driftless and also in scenarios where the number of GNSS satellites falls below four or even in case of total GNSS outage.

In the designed architecture, a GPS receiver and three supportive systems are integrated in the kinematic domain and in tracking and acquisition domain as well.

The GPS receiver is used as absolute reference to calibrate position and velocity provided by an IMU. This IMU, a Star Tracker and an orbital filter provide a GPS assistance not only in the tracking, but also in the acquisition process. The acquisition and tracking assistance then, allows acquiring, reacquiring and tracking weak signals quickly, even when they are only available for a short time interval. Every time they are available, the Star Tracker measurements are used to align and calibrate accurately the attitude outputted by the INS (integration of the gyros measurement). The integrated GNSS/INS/Star Tracker solution is finally fused via Kalman filtering with an on-board orbital forces model that takes into account the orbital trajectory constraints.

For the GNSS receiver, in the first step of our project, here presented, we have considered only the GPS constellation. Acquisition and tracking process have been developed initially for the only GPS L1 C/A, as the only civil signal in the L1 band currently provided by the full constellation. At the current step, for the acquisition process, the parallel code search (PCS) method and the full bit method have been adopted in order to maximize the coherent integration gain and reduce the computational burden. For the tracking process, we have implemented an Extended Kalmar Filter (EKF)-based carrier tracking and DLL tracking loops. The theoretical analysis and simulation results show that, by

using the implemented standalone GPS receiver, GPS L1 signals as low as 15 dB-Hz can be acquired and tracked successfully. Although the GPS L1 C/A sensitivity of 15 dB-Hz can ensure a GPS navigation solution (when the signals of 4 or more GPS satellites are available) most of the time during the considered trajectory, this results in a poor position accuracy. The use of a second frequency is required to remove ionosphere delays, responsible of possible considerable pseudorange errors, when the signals cross twice the atmosphere layers. Moreover tracking a modernized signal such as GPS L5 or Galileo E5b with a ten times smaller chipping rate than GPS L1 C/A or Galileo E1b reduces drastically the pseudorange tracking errors, which become very large for very weak signals. Due to the very big distance from the GPS satellites at the Moon altitude, the GDOP results to reach values higher than 1000 with a very strong penalizing impact on the final position accuracy. For this reason, the use of at least a second constellation is essential in order to improve the relative geometry between the receiver and the GNSS satellites (indeed the use of Galileo in addition to GPS can reduce considerably the GDOP). According to such results, in the second step of our project, we foresee to modify the GNSS receiver to make it capable to process the two GPS frequencies L1/L5 and the two Galileo frequencies E1/E5 in order to achieve few hundred meters of position accuracy at the Moon altitude, acceptable for a Moon Transfer Orbit (MTO) [3].

## ACKNOWLEDGMENTS

This research is being performed within the “WeakHEO” project, a proof of concept project between CAST Xi’an and EPFL ESPLAB.

## REFERENCES

1. S. Pace, “GPS in Space and Vision for Space Exploration”, Location 2006 Conference, Banglore, India, June 2006
2. W. A. Bamford, G. W. Heckler, G. N. Holt, M. C. Moreau, “A GPS Receiver for Lunar Missions”, ION NTM 2008, January 2008.
3. P. Silva, H. D. Lopes, T. R. Peres, J. S. Silva, J. Ospina, F. Cichocki, F. Dovis, L. Musumeci, D. Serant, T. Calmettes, I. Pessina, J. V. Perello, “Weak GNSS Signal Navigation to the Moon”, Nashville, US, ION GNSS+ , September 2013.
4. M.S. Braasch and M. Uijt de Haag, “GNSS For LEO, GEO, HEO and Beyond”, Advances in the astronautical sciences, pages 165-194, 2006.
5. V. Capuano, C. Botteron, P.-A. Farine, “GNSS Performances for MEO, GEO and HEO”, 64th International Astronautical Congress (IAC), Beijing, China, October 2013.
6. A. Dion, V. Calmettes, M. Bousquet, E. Boutillon, “Performances of a GNSS receiver for space-based applications”, Toulouse Space Show 2010.
7. V. Capuano, C. Botteron, P.-A. Farine, “GNSS to Reach the Moon”, 65th International Astronautical Congress (IAC), Toronto, Canada, October 2014.
8. http://www.navipedia.net/index.php/Ionosphere-free_Combination_for_Dual_Frequency_Receivers, last accessed on Sept. 4, 2014
9. http://www.gps.gov/systems/gps/space/, last accessed on July 15th 2014.
10. ICD-GPS-200F “Navstar GPS Space Segment/User Segment Interfaces”, 21 September 2011.
11. F. M. Czopek, S. Shollenberger, “Description and Performance of the GPS Block I and II L-Band Antenna and Link Budget”, ION GPS 1993.
12. E. D. Kaplan, C. J. Hegarty. “Understanding GPS: Principles and Applications”, Artech House, 2005.
13. F. van Diggelen, “A-GPS: Assisted GPS, GNSS and SBAS”, Artech house, 2009.
14. P. Groves, “Principles of GNSS, Inertial, and Multisensor Integrated Navigation Systems”, Artech House, 2nd edition, 2013.
15. Y. Wang, J. Tian, J. Leclère, C. Botteron, V. Capuano, P.-A. Farine, “An Efficient Time-frequency Algorithm for the Weak Signal Acquisition of Modernized GNSS Signals,” in proc. ION GNSS+ 2014, Tampa, Florida, USA, Sept. 8-12, 2014.
16. J. Leclère, C. Botteron, P.-A. Farine, “Comparison Framework of FPGA-Based GNSS Signals Acquisition Architectures”, IEEE Transactions on Aerospace and Electronic Systems (Volume 49 , Issue: 3 ), July 2013.
17. N.I. Ziedan, “GNSS receivers for weak signals”, Artech House, 2006.
18. L. Musumeci, F. Dovis, P. F. Silva, H.D. Lopes, J. S. Silva, “Design of a very High Sensitivity Acquisition System for a Space GNSS Receiver”, ION PLANS 2014.
19. O. Mancini, “Tutorial Precision Frequency Generation Utilizing OCXO and Rubidium Atomic Standards with Applications for Commercial, Space, Military, and Challenging Environments”, IEEE Long Island Chapter, March, 2004.
20. J.A. Del Peral-Rosado, “Kalman Filter-Based Architecture for Robust and High-Sensitivity Tracking in GNSS Receivers”, Satellite Navigation Technologies and European Workshop on GNSS Signals and Signal Processing (NAVITEC), 5th ESA Workshop, 2010.

21. "Star Camera". NASA. 05/04. Archived from the original on July 21, 2011. Retrieved 25 May 2012.
22. BCT-Nano-Star-Tracker-datasheet-version 1.1.
23. M. S. Grewal, "Global Navigation Satellite Systems, Inertial Navigation, and Integration", Wiley, 3rd edition, 2013.
24. R. Neville Thessin, "Atmospheric Signal Delay Affecting GPS Measurements Made by Space Vehicles During Launch, Orbit and Reentry", Master of Science in Aeronautics and Astronautics, Massachusetts Institute of Technology, 2005.